THE JOURNAL OF BIOLOGICAL CHEMISTRY VOL. 284, NO. 4, pp. 2053–2063, January 23, 2009

Molecular Basis for Enzymatic Sulfite Oxidation

HOW THREE CONSERVED ACTIVE SITE RESIDUES SHAPE ENZYME ACTIVITY[*S]

Received for publication, October 6, 2008, and in revised form, November 12, 2008 Published, JBC Papers in Press, November 12, 2008, DOI 10.1074/jbc.M807718200

Susan Bailey[‡1], **Trevor Rapson**[§], **Kayunta Johnson-Winters**[¶], **Andrei V. Astashkin**[¶], **John H. Enemark**[¶], **and Ulrike Kappler**[§2]

From the [‡]*Molecular Biophysics Group, Science and Technology Facilities Council Daresbury Laboratory, Warrington WA4 4AD, United Kingdom, the* [§]*Center for Metals in Biology, School of Molecular and Microbial Sciences, University of Queensland, Brisbane, Queensland 4072, Australia, and the* [¶]*Department of Chemistry, University of Arizona, Tucson, Arizona 85721*

Sulfite dehydrogenases (SDHs) catalyze the oxidation and detoxification of sulfite to sulfate, a reaction critical to all forms of life. Sulfite-oxidizing enzymes contain three conserved active site amino acids (Arg-55, His-57, and Tyr-236) that are crucial for catalytic competency. Here we have studied the kinetic and structural effects of two novel and one previously reported substitution (R55M, H57A, Y236F) in these residues on SDH catalysis. Both Arg-55 and His-57 were found to have key roles in substrate binding. An R55M substitution increased $K_{m(\mathrm{sulfite})(\mathrm{app})}$ by 2–3 orders of magnitude, whereas His-57 was required for maintaining a high substrate affinity at low pH when the imidazole ring is fully protonated. This effect may be mediated by interactions of His-57 with Arg-55 that stabilize the position of the Arg-55 side chain or, alternatively, may reflect changes in the protonation state of sulfite. Unlike what is seen for SDH^{WT} and SDH^{Y236F}, the catalytic turnover rates of SDH^{R55M} and SDH^{H57A} are relatively insensitive to pH (~60 and 200 s^{-1}, respectively). On the structural level, striking kinetic effects appeared to correlate with disorder (in SDH^{H57A} and SDH^{Y236F}) or absence of Arg-55 (SDH^{R55M}), suggesting that Arg-55 and the hydrogen bonding interactions it engages in are crucial for substrate binding and catalysis. The structure of SDH^{R55M} has sulfate bound at the active site, a fact that coincides with a significant increase in the inhibitory effect of sulfate in SDH^{R55M}. Thus, Arg-55 also appears to be involved in enabling discrimination between the substrate and product in SDH.

Sulfite-oxidizing enzymes protect cells against potentially fatal damage to DNA and proteins caused by exposure to sulfite, and consequently they are found in all forms of life (1). In bacteria, sulfite oxidation is often linked to energy-generating processes during chemolithotrophic growth on reduced sulfur compounds (2, 3), whereas both plant and vertebrate sulfite oxidases have been shown to detoxify sulfite arising from the degradation of methionine and cysteine and exposure to sulfur dioxide (4, 5).

All known sulfite-oxidizing enzymes belong to the same family of mononuclear molybdenum enzymes. Their active sites contain one molybdopterin unit per molybdenum atom, and these enzymes may also contain heme groups as accessory redox centers (6–9). Examples of different types of sulfite-oxidizing molybdoenzymes are the homodimeric plant sulfite oxidase, which does not contain a heme group and uses oxygen as its preferred electron acceptor (9), the homodimeric chicken and human liver sulfite oxidases (CSO[3] and HSO, respectively) (10), which are also able to use oxygen as an electron acceptor, and the bacterial sulfite dehydrogenase (SDH) isolated from the soil bacterium *Starkeya novella* (11, 12), which cannot donate electrons directly to oxygen. Each monomer of CSO and HSO contains a heme b center in addition to the molybdenum center, and the redox centers are located within separate, flexibly linked domains of the same protein subunit. In contrast, the bacterial enzyme is a heterodimer where each subunit of the enzyme contains one redox center. The molybdopterin cofactor is located in the larger 40.2-kDa SorA subunit, and the c-type heme is located in the smaller, 8.8-kDa SorB subunit (12). The SDH quaternary structure thus differs clearly from that of the human and chicken sulfite oxidases.

Crystal structures are available for plant sulfite oxidase, CSO, and the bacterial SDH (10, 11, 13–15) and have revealed molecular details of the sulfite-oxidizing enzymes. In the CSO structure, the mobile heme b domain occupies a position too removed from the molybdenum active site to mediate efficient electron transfer (10), and indeed the kinetics of this enzyme are known to be complicated by domain movements (16). In contrast, the bacterial SDH is a tight complex with strong electrostatic interactions between the subunits, and the close

* This work was supported, in whole or in part, by National Institutes of Health Grant GM-37773 (to J. H. E.). This work was also supported by a grant and fellowship from the University of Queensland (to U. K.), an Endeavor International Postgraduate Research Scholarship from the University of Queensland (to T. D. R.), and by the Science and Technology Facilities Council Daresbury Laboratory (for S. B.). This work was also supported by a Ruth L. Kirschstein National Service Award (to K. J.-W.). The costs of publication of this article were defrayed in part by the payment of page charges. This article must therefore be hereby marked "*advertisement*" in accordance with 18 U.S.C. Section 1734 solely to indicate this fact.

The atomic coordinates and structure factors (codes 2CA3 and 2CA4) have been deposited in the Protein Data Bank, Research Collaboratory for Structural Bioinformatics, Rutgers University, New Brunswick, NJ (http://www.rcsb.org/).

[S] The on-line version of this article (available at http://www.jbc.org) contains Figs. S1–S5 and Table S1.

[1] Supported during document preparation by the Director, Office of Science, Office of Basic Energy Sciences, of the United States Department of Energy under Contract DE-AC02-05CH11231. Present address: Lawrence Berkeley National Laboratory, Berkeley, CA 94720.

[2] To whom correspondence should be addressed. Tel.: 61-7-33652978; E-mail: u.kappler@uq.edu.au.

[3] The abbreviations used are: CSO, chicken liver sulfite oxidase; HSO, human liver sulfite oxidase; SDH, sulfite dehydrogenase; Bistris, 2-[bis(2-hydroxyethyl)amino]-2-(hydroxymethyl)propane-1,3-diol; Bistris propane, 1,3-bis-[tris(hydroxymethyl)methylamino]propane; ENDOR, electron-nuclear double resonance; WT, wild type.

approach of the redox centers (Mo–Fe distance 16.6 Å) allows for rapid electron transfer (11, 17) (Fig. 1, *A* and *B*).

Despite the overall structural differences of these proteins, the coordination geometries of the molybdenum active sites of these sulfite-oxidizing enzymes are nearly identical. The oxidized molybdenum center has a square pyramidal conformation, with three sulfur and two oxo ligands (18). Within this molybdenum center, the equatorial oxo ligand is proposed to be catalytically active, whereas the axial oxo ligand is not thought to participate directly in the reaction (Fig. 1*C*). During catalysis, the equatorial oxo ligand is transformed into a hydroxy/water ligand as a result of the reduction of the molybdenum center (Fig. 2), and it is in this form that it is generally observed in the CSO and SDH crystal structures.

SDH, CSO, and HSO show similarly high affinities for their substrate, sulfite, and several highly conserved residues surround the substrate-binding and molybdenum active site, namely Tyr-236 (all residues given in SDH numbering (11)), Arg-55, and His-57 (Fig. 1*D*). Both Arg-55 and Tyr-236 form hydrogen bonds to the catalytically active equatorial Mo-oxo group, whereas His-57 is positioned close to both Arg-55 and Tyr-236 (10, 11) (Fig. 1*D*). In addition, the crystal structure of the bacterial SDH shows that Arg-55 interacts directly with the second SDH redox center by hydrogen bonding to heme propionate-6 (Fig. 1*D*) (11).

As a result of the similarities in catalytic parameters and the structure of the active site, the bacterial SDH is a very good system for studies of enzymatic sulfite oxidation and especially the molecular basis for catalysis. Since this enzyme does not rely on domain movement for catalysis, it has a less complicated reaction mechanism than the vertebrate enzymes, which facilitates the interpretation of kinetic data, and it can be readily crystallized with both redox centers present in an electron transfer competent conformation. We have previously reported data on the structure, kinetics, EPR, and redox properties of a Y236F-substituted SDH (13). In addition to reduced turnover and substrate affinity, this substitution influences the reactivity of the SDH toward oxygen, turning SDH^{Y236F} essentially into an (albeit weak) sulfite oxidase. In order to further understand the roles of the conserved amino acids surrounding the molybdenum active site of sulfite-oxidizing enzymes, we have created two novel amino acid substitutions in the Arg-55 and His-57 residues present at the active site and have investigated their effect on catalytic and spectroscopic parameters of the bacterial SDH. We have also solved the crystal structures of the substituted enzymes, which have provided new insights into the conformation and plasticity of the active site of sulfite-oxidizing enzymes and how the conserved active site residues contribute to sulfite oxidation.

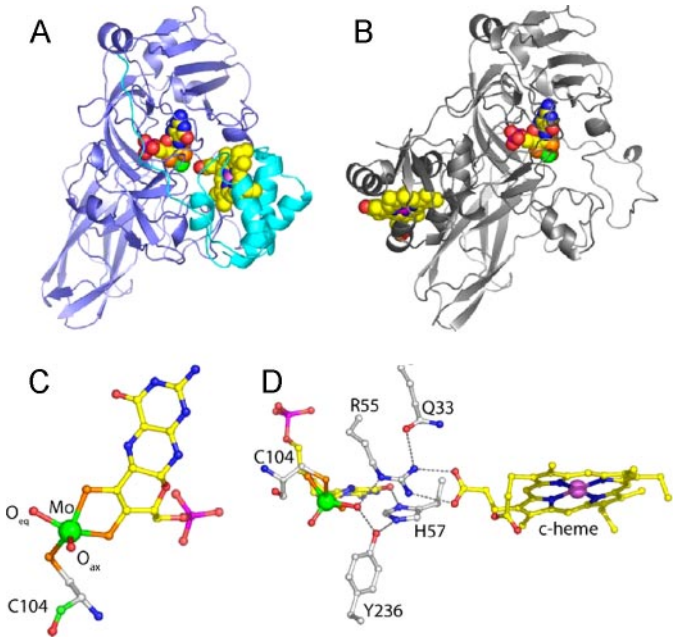

FIGURE 1. **Details of the crystal structure of wild type SDH and comparison with CSO.** *A*, *ribbon diagram* of the SDH heterodimer with the SorA and SorB subunits *colored blue* and *cyan*, respectively, and the redox cofactors in space-filling mode with the molybdenum atom *colored green* and the iron atom *colored violet*. *B*, *ribbon diagram* of a single subunit of CSO with the molybdopterin binding domain in the same orientation as SorA in *A*. The cytochrome domain of CSO is clearly in a different position with respect to the molybdenum cofactor than is seen for the cytochrome subunit of SDH. *C*, SDH molybdopterin cofactor demonstrating the geometry of the molybdenum ligands. The thiol ligands donated by the organic component of molybdopterin and the Cys-104 side chain, and the reactive oxygen ligand (O_{eq}) sit in the equatorial plane with the axial oxygen (O_{ax}) ligand at the *apex* of a *square pyramid*. Atoms are *colored* as follows: molybdenum (*green*), sulfur (*orange*), phosphorous (*magenta*), oxygen (*red*), nitrogen (blue), and carbon (*yellow* in the cofactor and *white* in the protein). *D*, hydrogen bonding network around the substrate binding site. The molybdopterin and heme cofactors are shown together with active site residues Cys-104, Arg-55, His-57, Tyr-236, and Gln-33. Figs. 1 and 4 were prepared using Pymol (37).

EXPERIMENTAL PROCEDURES

Molecular Biology—Standard methods were used throughout (19). The amino acid substitutions were created using the QuikChange mutagenesis kit (Stratagene) according to the manufacturer's instructions and the pSorex plasmid (20) as the mutagenesis template. Primers R55Mf (gac gcc ttc ttc gtg **atg** tac cat ctc gcc ggt), R55Mr (acc ggc gag atg gta **cat** cac gaa gaa ggc gtc), H57Af (ttc ttc gtg cgc tac **gcc** ctc gcc ggt ata ccg), and H57Ar (cgg tat acc ggc gag **ggc** gta gcg cac gaa gaa) were used to create an Arg-55 → Met and the His-57 → Ala substitution as described in Ref. 13. The presence of the substitutions in the plasmids pSorex-R55M and pSorex-H57A was confirmed by DNA sequencing, followed by subcloning of the expression construct into pRK415 as described in Ref. 20. The pRK415-based expression constructs pRK-sorexR55M and pRK-sorexH57A were transferred into *Rhodobacter capsulatus* 37B4 Δ*dorA* (21) by conjugation as in Ref. 20. Following conjugation, the expression plasmids were extracted from *R. capsulatus*, and the mutation was confirmed by DNA sequencing.

Protein Purification and Characterization—Recombinant protein was produced and purified as in Ref. 11. Metal analysis was performed by inductively coupled plasma mass spectrometry at the Acquire Center and the National Center for Environmental Toxicology, both at the University of Queensland. Protein determinations were carried out using the 2D Quant kit (GE Healthcare) or the BCA protein determination kit (BCA-1; Sigma), and polyacrylamide gels were prepared according to Ref. 22. Oxygen reoxidation experiments were carried out as described in Ref. 13.

TABLE 1
Data collection and refinement statistics

	R55M	H57A
Data collection		
Beamline	SRS 10.1	SRS 10.1
Wavelength (Å)	1.074	1.074
Resolution range (Å)	50–2.0	50–2.1
Unique reflections	34463	27649
Completeness (%)[a]	98.2 (89.1)	93.0 (83.8)
Multiplicity[a]	3.8 (2.7)	3.4 (2.0)
$I/s(I)$[a]	14.3 (3.8)	10.6 (2.1)
R_{merge}[b] (%)[a]	9.5 (28.8)	10.2 (41.8)
Refinement statistics		
Resolution range (Å)	30–2.0	20–2.1
R_{cryst}[c] (%)	16.3	14.7
R_{free}[d] (%)	20.7	20.1
Root mean square deviations from ideal geometry		
Bond lengths (Å)	0.016	0.012
Bond angles (degrees)	1.59	1.4
No. of water molecules	357	378

[a] Values in parentheses refer to the highest resolution shells of 2.07-2.0 Å and 2.21-2.1 Å.
[b] $R_{merge} = S_h S_i |(I_{hi} - I_h)| / S_h S_i |(I_{hi})$.
[c] $R_{cryst} = S|F_o - F_c|/\Sigma F_o$, where F_o and F_c are the observed and calculated structure factors, respectively.
[d] R_{free} was calculated with 5% of the data that had been excluded from refinement.

Crystallization and Solution of the SorAB^{R55M} and Sor^{H57A} Crystal Structures—Recombinant SDH^{R55M} and SDH^{H57A} were crystallized as previously described from 2.2 M ammonium sulfate, 2% polyethylene glycol 200, 1 M HEPES, pH 7.4 (11), and crystals were cryocooled to 100 K within 5 days of setting up crystallization trials. Data were collected on beamline 10.1 of the SRS, Daresbury Laboratory. Data were processed and scaled using Mosflm/SCALA (23), and further analysis used programs from the CCP4 suite (24). The crystal structure was refined with the program REFMAC (25), using the SDH^{WT} structure (11) (Protein Data Bank code 2BlF) as the starting point, and inspection of the model and electron density maps was carried out using the program O (26). Data collection, processing, and refinement statistics are shown in Table 1. The final models comprise residues 1–373 of the SorA subunit, residues 1–81 of the SorB subunit, one molybdenum cofactor (Moco), one c-type heme, one or two sulfate ions, and water molecules. The structures have good stereochemistry with 99.5% of the residues in the most favored and additionally allowed regions and no residues in disallowed regions of the Ramachandran plot, as defined by PROCHECK (27).

For the SDH^{R55M} structure, weighted difference Fourier maps calculated with coefficients $mF_o - DF_c$ showed a strong negative peak on the molybdenum atom, which suggested that this atom is not fully occupied. This situation has already been observed for the SDH^{Y236F} structure (13), and the same procedure was used to estimate the molybdenum occupancy. The occupancy of the molybdenum was estimated at 50%. Further refinement with the molybdenum occupancy set appropriately resulted in a reasonable B-factor for this atom, similar to that of surrounding atoms, and no significant residual difference density. In the case of the SDH^{H57A} structure, the molybdenum appears fully occupied.

Enzyme Assays—Routine enzyme assays were carried out at 25 °C using 20 mM Tris acetate buffer, pH 8, 2 mM sulfite, 0.04 mM cytochrome *c* (horse heart; catalog number C7752; Sigma) and a suitable amount of sulfite dehydrogenase (0.1–0.2 nmol, depending on the variant studied) (12, 13), using either a Hitachi UV3000 double beam spectrophotometer or a Cary 50 spectrophotometer (Varian). The reaction was started by the addition of sulfite, and the reduction of cytochrome *c* was monitored at 550 nm. Both sulfite and cytochrome *c* solutions were prepared fresh each day. Studies of enzyme stability as a function of pH were conducted by preincubating a concentrated sample of purified enzyme at the specified pH value. Samples were removed from these solutions at various time intervals, and enzyme activities were immediately determined using the standard assay at pH 8.0. The normal time scale of an SDH assay is between 90 and 120 s, the preincubation experiments were carried out for up to 15 min. For determination of $K_{m(sulfite)(app)}$ values, the amount of sulfite added to the assay was varied and sulfite concentrations between ~0.2 and 10 K_m were used. All assays were carried out in triplicate. Buffer systems used were 20 mM Bistris acetate (pH 6.0 and 6.5), 20 mM Tris acetate (pH 7.0–8.5), 20 mM glycine (pH 9.0–10.0), similar to the systems used in studies of CSO (28) and HSO (29), except for SDH^{R55M}, where all buffers used were 20 mM Tris acetate. Very high concentrations of sulfite (>20 mM) were found to inhibit the SDH reaction. Kinetic constants were derived by direct nonlinear regression using SigmaPlot 9.0 (SysStat Inc.).

The effect of sulfate on SDH activity (SDH^{WT} and SDH^{R55M}) was investigated in two ways: 1) increasing amounts of sulfate were added to standard SDH assays, and the changes in reaction velocity observed; 2) to determine the effect of sulfate on $K_{m(sulfite)(app)}$ and $k_{cat(app)}$, these parameters were determined in the presence of 0, 10, 30, and 60 mM sodium sulfate, as described above.

Non-steady-state parameters for the reductive half-reaction of wild type and mutant SDH were determined on an SX18.MV Stopped Flow apparatus (Applied Photophysics) at 10 °C. The lowering of the temperature was necessary, since the $k_{red(heme)}$ values observed for the wild type enzyme were approaching the detection limits of the apparatus. Experiments were carried out using 20 mM buffers and a final concentration of 1.1 μM purified, oxidized sulfite dehydrogenase (except for SDH^{H57A}, where a 0.4 μM enzyme solution was used), and the reaction was monitored at 418 nm. Sulfite concentrations were varied between 2.5 and 16,000 μM (final concentration) as appropriate for each enzyme used. Parameters for SDH^{Y236F} could not be determined, since this enzyme can be reoxidized by molecular oxygen, and accessories for anaerobic work were not available. Similarly, only a core data set could be determined for SDH^{H57A} due to the scarcity of the protein. $K_{d(sulfite)}$ and $k_{red(heme)}$ were determined by direct nonlinear fitting of the data.

EPR—EPR samples for SDH^{WT} and SDH^{R55M} were prepared in buffers containing 100 mM Bistris propane, pH 7.0, whereas the SDH^{H57A} sample was prepared in 100 mM Bistris (pH 5.8). The pH of the buffer was adjusted using NaOH or acetic acid to give the required pH. Approximately 1 mg of protein was reduced with a 20-fold excess of sodium sulfite and immediately frozen in liquid nitrogen. The continuous wave EPR spectra were recorded on a Bruker ESP-300E spectrometer at 77 K using the experimental parameters given in the legend for Fig. 4. Pulsed electron-nuclear double resonance (ENDOR) experi-

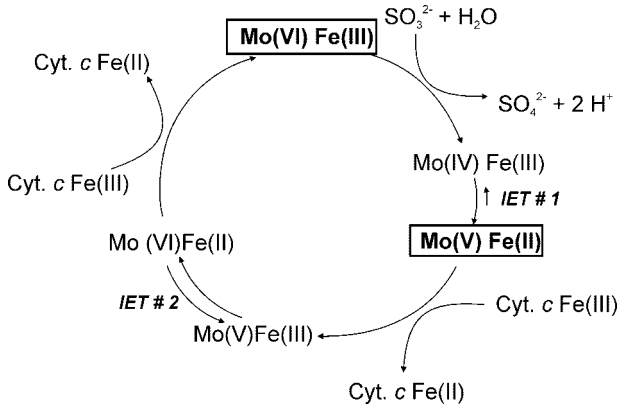

FIGURE 2. **Proposed reaction mechanism for *S. novella* sulfite dehydrogenase.** The reaction is shown in terms of the redox states of the molybdenum and heme centers present in the enzyme. Shown in *boldface type* and *boxed* are the stable redox states of the *S. novella* SDH. *Cyt. c*, a mitochondrial type cytochrome c_{550} (*e.g.* horse heart or *S. novella* cytochrome c_{550}) that can act as the external electron acceptor.

TABLE 2

Kinetic parameters of the SorAB sulfite dehydrogenase (SDH^{WT}) from *S. novella*

pH	$K_{m(\text{sulfite})}$	k_{cat}	$k_{\text{cat}}/K_{m(\text{sulfite})}$
	mM	s^{-1}	$M^{-1}\ s^{-1}$
6.0	$0.6 \times 10^{-3} \pm 9.5 \times 10^{-5}$	63.5 ± 2.2	1.06×10^{8}
6.5	$1.1 \times 10^{-3} \pm 0.14 \times 10^{-3}$	86.2 ± 2.2	7.55×10^{7}
7.0	$3.7 \times 10^{-3} \pm 0.45 \times 10^{-3}$	158.8 ± 4.5	4.27×10^{7}
7.5	$7.1 \times 10^{-3} \pm 0.82 \times 10^{-3}$	293.4 ± 7	4.03×10^{7}
8.0	$2.2 \times 10^{-2} \pm 0.26 \times 10^{-2}$	345.3 ± 11	1.53×10^{7}
8.5	$8.6 \times 10^{-2} \pm 0.85 \times 10^{-2}$	410 ± 11	4.88×10^{6}
9.0	0.324 ± 0.029	519 ± 11	1.5×10^{6}
9.5	1.66 ± 0.18	431 ± 16	2.51×10^{5}
10.0	3.389 ± 0.44	23.7 ± 1.3	6.77×10^{3}

ments were performed on a home-built K_a-band (26–40 GHz) pulsed EPR spectrometer (30).

RESULTS

Catalytic Properties of the Wild Type Sulfite Dehydrogenase—To date, only catalytic parameters determined at pH 8 and pH 6 have been reported for SDH^{WT} (13). In order to be able to fully assess the impact of substitutions of active site amino acids on the SDH-catalyzed reaction (Fig. 2), we first determined a complete set of $K_{m(\text{sulfite})(\text{app})}$ and $k_{\text{cat}(\text{app})}$ values for SDH^{WT} between pH 6 and 10 (Table 2 and Fig. 3).

To ensure that observations made were not due to artifacts caused by inactivation of the sulfite dehydrogenase upon exposure to extreme pH values, the stability of the wild type and mutant enzymes was determined between pH 6 and 10 as a function of time. No significant loss of activity was observed (Table S1).

The apparent $K_{m(\text{sulfite})}$ values for SDH^{WT} decrease with decreasing pH to a value of 0.0006 mM at pH 6 and increase markedly above pH 8.5 to a maximum of 3.4 mM at pH 10. A similar behavior with strong increases of $K_{m(\text{sulfite})(\text{app})}$ above pH 8.5 has been reported for both CSO ($K_{m(\text{sulfite})}$ 0.01–0.118 mM, pH 6–10) (28) and HSO ($K_{m(\text{sulfite})}$ 0.0012–0.067 mM, pH 6–10) (29). The change in $K_{m(\text{sulfite})(\text{app})}$ seen in SDH^{WT} at higher pH values, however, is more than 1 order of magnitude larger than that seen for the two vertebrate enzymes. This characteristic change in substrate affinity at higher pH has been suggested to be indicative of a preference of the enzyme for hydrogen sulfite (29), HSO_3^-, which has a pK_a value of pH 7.2 (31). At pH 8.5 and higher, the protonated form of the substrate molecule can be expected to be present in only very small amounts (Fig. 3*A*).

The $k_{\text{cat}(\text{app})}$ values for SDH increase up to pH 9.0 where a value of 519 ± 11 s^{-1} is reached, after which turnover numbers decline rapidly toward 23.7 ± 1.3 s^{-1} at pH 10 (Table 2 and Fig. 3*C*). CSO exhibits the same behavior with $k_{\text{cat}(\text{app})}$ increasing up to 119 s^{-1} at pH 9.0 (28), however, HSO $k_{\text{cat}(\text{app})}$ showed only a single pK_a at low pH and reached a steady maximal value of ~25 s^{-1} at pH 7.5 and higher (29).

The data in Table 2 were fitted to a bell-shaped profile as described in Ref. 13, and pK_a values of pH 7.5 and pH 9.7 were derived. These pK_a values are slightly different from previously reported values obtained under standard assay conditions (2 mM sulfite), where maximal SDH activity is observed at pH 8.0–8.5 with apparent pK_a values of pH 7.6 and pH 9.4 (12, 13) (Fig. S1). The new data presented here clearly show that the strong increase in $K_{m(\text{sulfite})(\text{app})}$ above pH 8.5 shapes the activity profile and causes the apparent decrease in activity previously observed under standard conditions, since sulfite is no longer present in saturating concentrations.

As judged by the magnitude of the second order rate constants, SDH is a highly efficient enzyme that operates close to the limits imposed by substrate diffusion, with apparent $k_{\text{cat}}/K_{m(\text{sulfite})(\text{app})}$ values in the range of 10^7 M^{-1} s^{-1} at pH 8.0 and below (Table 2 and Fig. 3*E*). Plots of $k_{\text{cat}}/K_{m(\text{sulfite})(\text{app})}$ *versus* pH have an S-shaped profile with a pK_a of pH 7.0 ± 0.14.

Catalytic Properties of Y236F-substituted Sulfite Dehydrogenase—Three crucial and strictly conserved residues, Tyr-236, Arg-55, and His-57, are found close to the molybdenum active site of sulfite-oxidizing enzymes and have been shown to interact with the molybdenum center (11, 13). Tyr-236 forms a hydrogen bond with the reactive equatorial oxo-group of the molybdenum center, an interaction that is disrupted by the Y236F substitution. We have previously reported catalytic parameters of SDH^{Y236F} at pH 6.0 and pH 8.0 (13). A full set of catalytic parameters for this enzyme is set out in Table 3. The Y236F substitution leads to an increase in $K_{m(\text{sulfite})(\text{app})}$ values by a factor of ~5–7. Thus, Tyr-236 appears to have a moderate influence on substrate binding or the stability of the enzyme-substrate complex. This latter effect may also be mediated by changes in the ligand environment of the molybdenum center caused by the loss of the hydrogen bond between Tyr-236 and the equatorial molybdenum oxo-group, although our earlier study failed to show any changes in the molybdenum redox potential (13). For SDH^{Y236F}, the overall shape of the $k_{\text{cat}(\text{app})}$ *versus* pH plot is similar to that seen for SDH^{WT}, and the optimum pH for activity is pH 9.0 in both cases (Fig. 3*D*). However, in SDH^{Y236F}, $k_{\text{cat}(\text{app})}$ is lowered to about 13% of the SDH^{WT} activity between pH 7.5 and 9.5, with SDH^{Y236F} activities at the extremes of the pH scale being matched more closely to that of SDH^{WT}. It therefore appears that in addition to its important role in regulating the activity of sulfite-oxidizing enzymes toward oxygen (13), Tyr-236 also affects enzyme turnover.

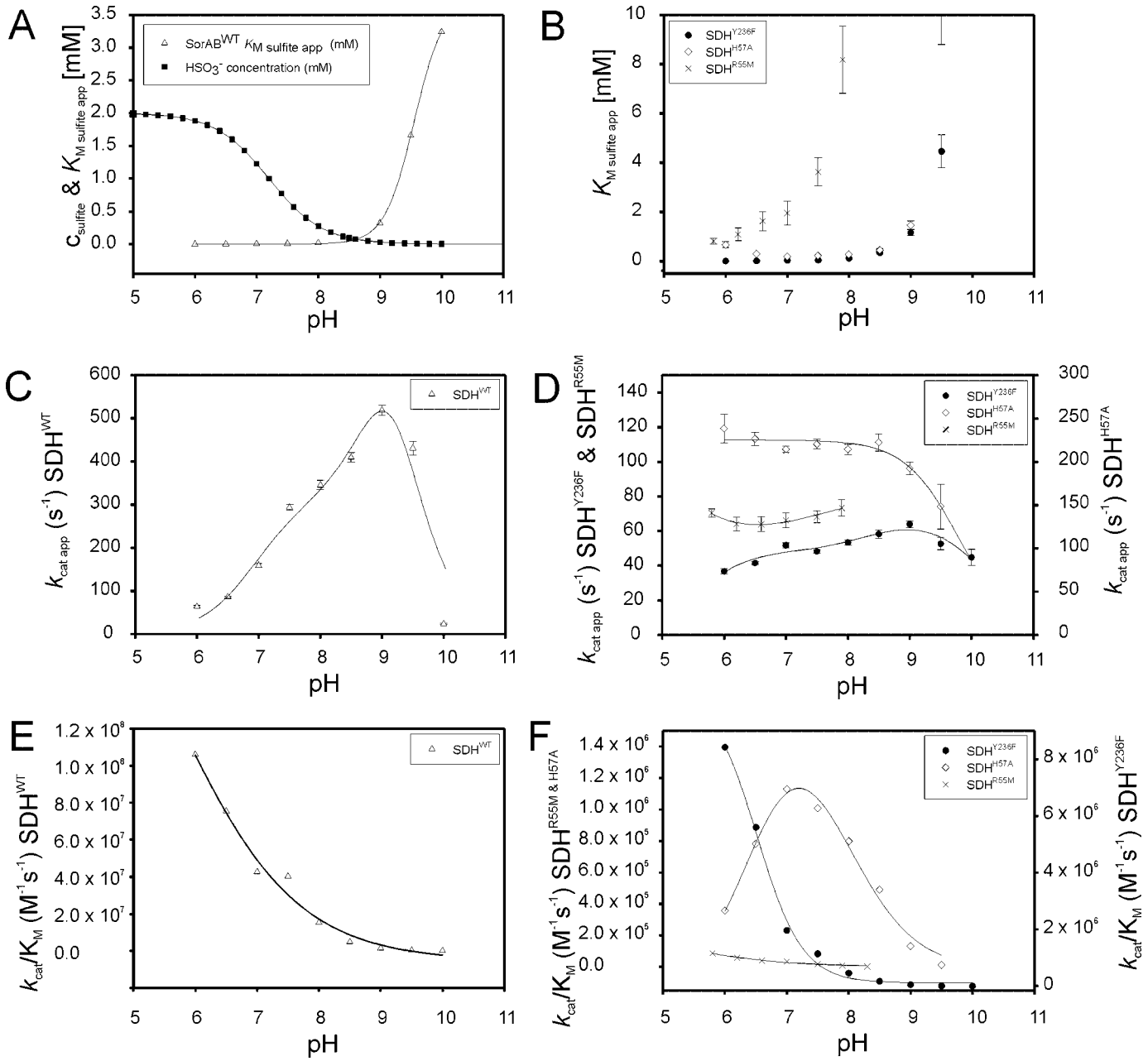

FIGURE 3. **Influence of pH on the kinetic parameters of SDH^{WT} and its substituted forms.** *A*, plot of $K_{m(sulfite)(app)}$ for SDH^{WT} and sulfite speciation *versus* pH; *B*, plot of $K_{m(sulfite)(app)}$ *versus* pH for SDH^{R55M} (×), SDH^{Y236F} (●), and SDH^{H57A} (◇); *C*, plot of $k_{cat(app)}$ *versus* pH for SDH^{WT}; *D*, plot of $k_{cat(app)}$ *versus* pH for SDH^{R55M} (×), SDH^{Y236F} (●), and SDH^{H57A} (◇); *E*, plot of $k_{cat}/K_{m(sulfite)}$ *versus* pH SDH^{WT}; *F*, plot of $k_{cat}/K_{m(sulfite)}$ *versus* pH for SDH^{R55M} (×), SDH^{Y236F} (●), and SDH^{H57A} (◇).

Catalytic Properties of the R55M- and H57A-substituted Sulfite Dehydrogenases—In order to investigate the influence of the other two strictly conserved residues on SDH activity, we created substitutions in both Arg-55 and His-57. The molybdenum content of the two novel substituted proteins was determined by inductively coupled plasma mass spectrometry. The molybdenum content of the SDH^{R55M} was between 60 and 70%, whereas SDH^{H57A} contained ~75–83% molybdenum, both being indicative of a high proportion of active enzyme in the respective preparations. Since SDH^{R55M}, like the previously described SDH^{Y236F}, carries a substitution very close to the molybdenum active site, we investigated whether the substitution of Arg-55 also leads to an increased reactivity toward oxygen. However, within experimental error, the air reoxidation rates for SDH^{R55M} were the same as those determined for SDH^{WT} (13).

In steady-state assays, the substitution of a Met residue for Arg-55 resulted in a variant SDH characterized by two key features (Table 3): an increase of $K_{m(sulfite)(app)}$ by 2–3 orders of magnitude relative to SDH^{WT} and, interestingly, a nearly invariant value for $k_{cat(app)}$ (~65 s^{-1}) between pH 6 and pH 8. These results clearly point to an important role for Arg-55 in substrate binding and/or the stabilization of the enzyme-substrate complex as well as a role in shaping the characteristic SDH activity profile via influencing enzyme turnover.

TABLE 3

Kinetic parameters of substituted SorAB sulfite dehydrogenases, SDH^{Y236F}, SDH^{R55M}, and SDH^{H57A}

Square brackets denote values for which insufficient data points could be obtained due to the high sulfite concentrations needed to achieve saturating sulfite concentrations.

pH	Kinetic parameters		
	$K_{m(\text{sulfite})}$	k_{cat}	$k_{cat}/K_{m(\text{sulfite})}$
	mM	s^{-1}	$M^{-1}\,s^{-1}$
SDH Y236F			
6.0	$0.004 \pm 0.6 \times 10^{-3}$	36.8 ± 1.5	8.42×10^6
6.5	$0.007 \pm 0.6 \times 10^{-3}$	41.6 ± 0.8	5.60×10^6
7.0	0.026 ± 0.0032	51.8 ± 1.5	1.97×10^6
7.5	0.042 ± 0.0041	48.3 ± 1	1.14×10^6
8.0	0.114 ± 0.0135	53.4 ± 1.6	4.61×10^5
8.5	0.332 ± 0.0447	58.3 ± 2.4	1.73×10^5
9.0	1.155 ± 0.1166	64 ± 2	5.45×10^4
9.5	4.456 ± 0.6693	52.7 ± 3.5	1.16×10^4
10.0	15.487 ± 2.8	44.8 ± 4.7	2.84×10^3
SDH R55M			
5.8	0.812 ± 0.114	70.5 ± 2.4	8.68×10^4
6.2	1.087 ± 0.26	64.0 ± 3.9	5.89×10^4
6.6	1.63 ± 0.39	64.0 ± 4.3	3.93×10^4
7.0	1.95 ± 0.49	66.3 ± 4.2	3.4×10^4
7.5	3.62 ± 0.57	68.3 ± 3.3	1.89×10^4
7.9	8.17 ± 1.37	73.4 ± 4.8	8.98×10^3
8.3	[33.27 ± 7.5]	[109.88 ± 15.04]	[3.3×10^3]
SDH H57A			
6.0	0.667 ± 0.12	238.8 ± 16.5	3.58×10^5
6.5	0.29 ± 0.003	226.5 ± 7.6	7.82×10^5
7.0	0.189 ± 0.001	214.5 ± 3.7	1.13×10^6
7.5	0.22 ± 0.002	220.5 ± 5.6	1.01×10^6
8.0	0.27 ± 0.003	214.6 ± 6	7.99×10^5
8.5	0.452 ± 0.06	222.4 ± 9.9	4.92×10^5
9.0	1.46 ± 0.16	192.5 ± 7.5	1.32×10^5
9.5	12.2 ± 3.4	148.4 ± 25.8	1.22×10^4

The plot of $K_{m(\text{sulfite})(\text{app})}$ *versus* pH still shows the characteristic steep increase at higher pH values, previously observed for SDH^{WT} and SDH^{Y236F}. However, we note that care should be taken in the interpretation of the higher pH catalytic data for SDH^{R55M}, since these could not be reliably determined above pH 8 due to the large amounts of sulfite needed to saturate the reaction (around 10 mM at pH 6 and well over 35 mM at pH 8), as a result of the large values for $K_{m(\text{sulfite})(\text{app})}$. SDH^{R55M} appears to gain activity at lower pH values when assayed under standard conditions with 2 mM sulfite present, resulting in an activity profile with a single apparent pK_a and maximal activity at pH 6 or below (Fig. S1).

Compared with SDH^{R55M}, the changes in the catalytic parameters seen following a H57A substitution were more subtle (Table 3). The $k_{cat(app)}$ values were found to be fairly constant over the pH range 6–9, although SDH^{H57A} showed a higher level of activity at ~200 s^{-1} than SDH^{Y236F} and SDH^{R55M} over the pH ranges measured. Indeed, at pH 7 and below SDH^{H57A}, $k_{cat(app)}$ rates are higher than those of the wild type enzyme.

Substitution of His-57 with alanine also lowers substrate affinity, as demonstrated by the increase in $K_{m(\text{sulfite})(\text{app})}$ values. The most notable observation, however, was that the pH profile for $K_{m(\text{sulfite})(\text{app})}$ reaches a minimum at pH 7 (0.189 ± 0.001 mM), and values increase clearly below that pH to a value of 0.667 ± 0.12 mM at pH 6. At pH 8 and above, $K_{m(\text{sulfite})(\text{app})}$ was increased slightly (by factors of ~5–10) relative to SDH^{WT}, indicating that although it is removed from the molybdenum center, His-57 has a role in substrate binding. None of the wild type and substituted sulfite-oxidizing enzymes (both SDH and CSO/HSO type) studied to date show a similar increase of $K_{m(\text{sulfite})(\text{app})}$ at low pH, making SDH^{H57A} a unique target for further studies into catalysis in these enzymes. Our data suggest that the protonation of the His-57 residue (pK_a ~ 6.04) (32) at lower pH values may have a major role in maintaining the high affinity of sulfite-oxidizing enzymes for sulfite (or hydrogen sulfite) at pH values below 7.

TABLE 4

Non-steady state kinetic parameters for the reductive half-reaction of the SDH^{WT} and SDH^{R55M} sulfite dehydrogenases

Data were collected at 418 nm and 10 °C. Square brackets denote values for which insufficient data points could be obtained due to the high sulfite concentrations needed to achieve saturating sulfite concentrations.

pH	Kinetic parameters		
	$K_{d(\text{sulfite})}$	$k_{red(\text{heme})}$	$k_{red(\text{heme})}/K_{d(\text{sulfite})}$
	mM	s^{-1}	$M^{-1}\,s^{-1}$
SDH WT			
6	0.0032 ± 0.0003	730 ± 10	2.25×10^8
6.5	0.0036 ± 0.0002	847 ± 10	2.39×10^8
7	0.0014 ± 0.0001	782 ± 16	5.58×10^7
7.5	0.0031 ± 0.0003	677 ± 20	2.18×10^7
8	0.0087 ± 0.0007	776 ± 22	8.89×10^6
8.5	0.412 ± 0.029	829 ± 32	2.01×10^6
9	1.183 ± 0.094	731 ± 20	6.18×10^5
9.5	3.811 ± 0.75	674 ± 45	1.77×10^5
SDH R55M			
5.5	4.53 ± 0.51	746 ± 34	1.65×10^5
6	6.48 ± 0.68	662 ± 31	1.02×10^5
7	[22.8 ± 4.5]	[240 ± 32]	[1.05×10^4]

Non-steady-state Parameters of the Reductive Half-reaction of SDH—pH-dependent changes in steady-state kinetic parameters may not always directly reflect a change in the molecular properties of the enzyme under study. To ascertain whether this was the case here, the non-steady-state parameters for the reductive half-reaction of SDH^{WT}, SDH^{R55M}, and SDH^{H57A} were determined (Table 4 and Fig. S2). All experiments were carried out at 10 °C to keep reaction rates well within the specification of the instrument used.

For SDH^{WT} $K_{d(\text{sulfite})}$ decreased with decreasing pH in the same way as the $K_{m(\text{sulfite})(\text{app})}$ values determined in steady-state assays. Overall, $K_{d(\text{sulfite})}$ values were slightly higher than the corresponding apparent $K_{m(\text{sulfite})}$ values, which may be due to the different temperatures at which the assays were carried out (Table 4). In contrast, $k_{red(\text{heme})}$, which reflects the SDH reaction rate up to the formation of the stable, Mo(V)Fe(II), the two-electron reduced form of SDH was nearly invariant with pH up to pH 9 at ~740 s^{-1}, which differs from the behavior observed for k_{cat} but is similar to what has been reported for vertebrate sulfite oxidases (28, 29). As already pointed out for CSO (28), the difference in the behavior of k_{cat} and $k_{red(\text{heme})}$ indicates that processes unrelated to the reductive half-reaction contribute to the kinetic barrier to catalysis. Interestingly, both SDH^{R55M} and SDH^{H57A} have a nearly pH-invariant k_{cat} similar to the SDH^{WT} $K_{d(\text{sulfite})}$ profile.

A close correlation between the behavior of the steady-state kinetic parameters and K_d sulfite was also observed for both SDH^{R55M} and SDH^{H57A} (Table 4 and Fig. S2). Due to the very low affinity of SDH^{R55M} for the substrate, sulfite, meaningful data could only be determined at pH 5.5 and 6, with the pH 7 data set clearly demonstrating the extreme increase in K_d sulfite at that pH.

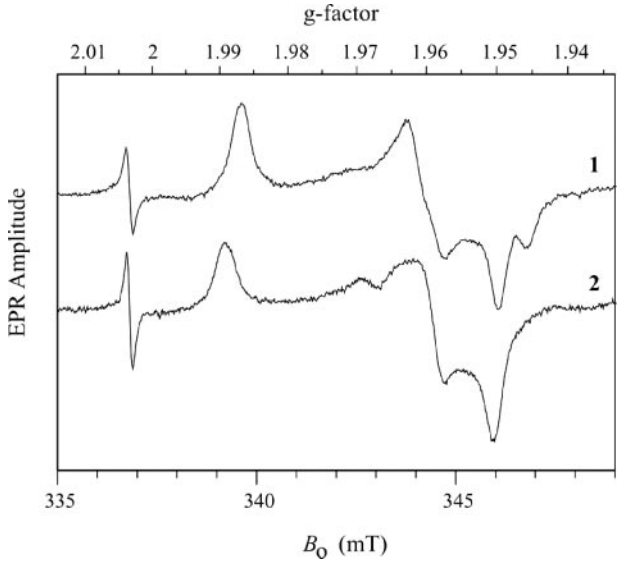

FIGURE 4. **Continuous wave EPR spectra of SDH forms.** *Trace 1*, SDH^{H57A} at pH 5.8; *trace 2*, SDH^{R55M} at pH 7.0. Experimental conditions were as follows: ν_{mw} = 9.444 GHz; modulation amplitude = 0.1 millitesla; microwave power = 0.2 milliwatt; temperature = 77 K. The *narrow line* at g = 2.0036 is the signal of the DPPH standard.

Only limited data could be collected for SDH^{H57A}, since preparations of this protein yield much less enzyme than those of either SDH^{R55M} or SDH^{WT}. However, a plot of reaction rates *versus* sulfite concentrations at different pH values clearly shows that, similar to what was observed with the apparent $K_{m(sulfite)}$ values for this enzyme, $K_{d(sulfite)}$ reaches a minimum at pH 7. These observations strongly suggest that the kinetic effects observed in the substituted SDH proteins are a direct result of the pH dependence of elementary steps in the enzyme's mechanism.

Characterization of the Molybdenum Centers of SDH^{R55M} and SDH^{H57A}—The X-band continuous wave EPR spectra for SDH^{R55M} and SDH^{H57A} are shown in Fig. 4. For SDH^{R55M} (trace 2) the principal g values (g_X, g_Y, and g_Z = 1.951, 1.960, and 1.989) are similar to those for SDH^{WT} (g_X, g_Y, and g_Z = 1.9541, 1.9661, and 1.9914) (12, 13). For SDH^{H57A} at low pH (*trace 1*), the spectrum shows a well defined low field turning point (g_Z = 1.987), but the intermediate and high field regions are each split into two components. One explanation of these features is to attribute them to two structurally different Mo(V) centers with different principal g values. On the other hand, since the amplitudes of these components are similar, the question may arise whether they result from hyperfine splittings at g_X and g_Y. It is easy to distinguish between these two possibilities by recording an EPR spectrum at a different microwave band in order to see if the positions of the EPR features scale in proportion with the microwave frequency. Such measurements were performed at the microwave K_a-band (~30 GHz; Fig. S3), and it was established that the EPR spectral features belong to two species, I and II, with different sets of principal g values (g_X, g_Y, and g_Z = 1.950, 1.962, and 1.987 and g_X, g_Y, and g_Z = 1.946, 1.959, and 1.987, respectively, with g_Z being the same for both centers.

The g values of Species I are similar to those of high pH SO or SDH^{WT} (33), but the second set is somewhat different, and the question arises whether this change could be caused by some alteration of the exchangeable equatorial ligand in Species II. In order to answer this question, ENDOR measurements at different EPR positions were performed (Fig. S4). The ENDOR spectra obtained (Fig. S4) exhibit broad shoulders with a splitting of up to 8 MHz, centered about the central sharp peaks. These shoulders were shown to arise from the OH ligand proton in the high pH form of sulfite-oxidizing enzymes (34). Thus, the current ENDOR measurements (Fig. S4) have shown that the characteristic features of an equatorial OH-ligand proton are present with unchanged amplitude even at the highest field turning point that is solely contributed by Species II. This observation means that the exchangeable equatorial ligand is the same for both species and that it is unlikely to be responsible for the variability of the principal g values. Rather, the interactions of Species I and II of SDH^{H57A} with the active site surroundings somehow perturb the D-orbitals of Mo(V) slightly differently. The individual structures giving rise to species I and II are likely to be very similar to one another. However, the overlap of their signals makes it impossible to investigate them separately by pulsed EPR.

Structure of SDH^{R55M}—The Arg-55 side chain of SDH^{WT} occupies an important position close to the substrate binding site, where it makes hydrogen bonds to the equatorial oxo ligand of the molybdenum, to Gln-33 OE1, and a nearby water molecule. It also forms a salt bridge, comprising two hydrogen bonds, with propionate-6 of the heme moiety of the cytochrome subunit (Fig. 1*D*), which effectively locks the propionate group into position (11). The guanidinium group of Arg-55 stacks against the imidazole ring of His-57, potentially forming a long hydrogen bond (3.5 Å) and is also found in proximity (3.8 Å) to Tyr-236.

In the crystal structure of SDH^{R55M}, the side chain of Met-55 does not occupy the same position as Arg-55 in the SDH^{WT} structure; instead, it is bent away, packing into a small cavity between the side chains of Leu-121 and Gln-33. The space occupied by Arg-55 in the wild type enzyme appears to be largely empty in SDH^{R55M}, and a water molecule that is hydrogen-bonded to Arg-55 in SDH^{WT} and is in a position to interact with the substrate/product is missing in SDH^{R55M} (Fig. 5, *A* and *B*). A small movement of the Gln-33 side chain causing a 1.0-Å shift in the position of the Gln-33 OE1 may be due either to the loss of interaction with Arg-55, to the position of Met-55, which is located 3.0 Å from Gln-33 OE1 and potentially forms an S–O hydrogen bond, or to the loss of the water molecule associated with Arg-55.

In SDH^{R55M}, the interactions with the heme propionate-6 moiety are also disrupted, and as a result, the propionate displays greater mobility, confirming our earlier suggestions that Arg-55 contributes to the positioning of the propionate-6 moiety (11). Propionate-6 has been modeled in two conformations, with ~70% of this group remaining in the same position as in SDH^{WT} and ~30% rotated around the C3D-CAD bond, displacing a nearby water molecule (Fig. 5).

Structure of SDH^{H57A}—The His-57 side chain of SDH^{WT} is positioned at the side of the substrate binding site between the side chains of Arg-55 and Tyr-236, with His-57 NE2 forming a hydrogen bond to Tyr-236 OH. His-57 also contributes to the

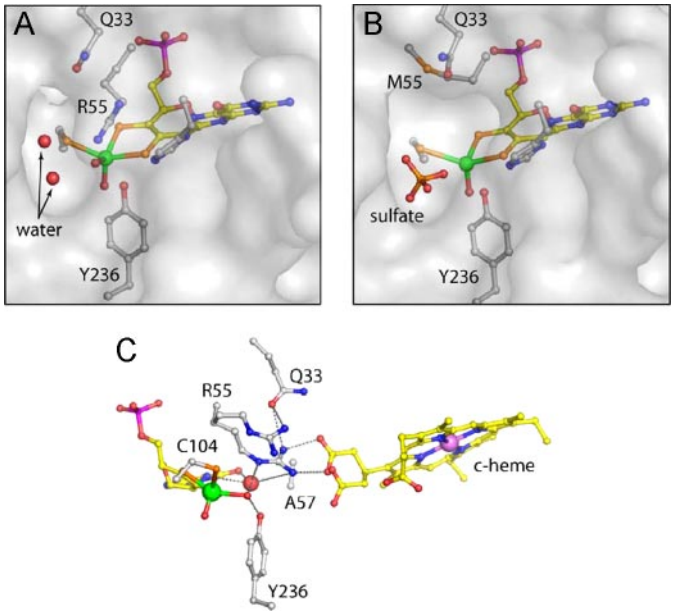

FIGURE 5. **Active site structures of SDH^{R55M} and SDH^{H57A}.** *A* and *B* show a transparent surface at the substrate binding sites of SDH^{WT} and SDH^{R55M}, respectively. The water-filled cavity adjacent to the equatorial oxygen is larger in the mutated enzyme and is occupied by a sulfate ion. *C*, hydrogen bonding network around the active site of SDH^{H57A} in a similar view as SDH^{WT} in Fig. 1*D*. The two alternative positions for Arg-55 and the heme propionate group are shown. An additional water molecule occupies a site close to the pterin, and fulfills potential hydrogen bond contacts.

molybdopterin binding site via a hydrogen bond from His-57 ND1 to molybdopterin O4 (11, 13) (Fig. 1*D*).

The structure of SDH^{H57A} confirms the substitution of His-57 with the smaller alanine and identifies an additional water molecule that sits close to the position occupied by the imidazole ring in SDH^{WT}. This water is at a distance to form hydrogen bonds with both N5 and O4 of the molybdopterin. In contrast with the SDH^{Y236F} and SDH^{R55M} active site mutants of SDH, the molybdenum site is fully occupied, probably reflecting the more distant position of His-57 from the molybdenum center and the absence of a direct link to a molybdenum ligand. One consequence of the H57A substitution indicated by the difference electron density appears to be increased mobility of both the Arg-55 side chain and the interacting propionate-6 side chain of the heme. These latter side chains have both been modeled in two alternative conformations in this structure; ~65% is in the same position as in SDH^{WT}, whereas 35% occupies an alternative position in which the salt bridge is disrupted (Fig. 5*C* and Fig. S5). These two alternative conformations may also account for the two different EPR signals for SDH^{H57A} (Fig. 4; see above).

The data, together with the structure of SDH^{Y236F}, reveal that both Tyr-236 and His-57 are necessary to stabilize Arg-55 in a position for optimal hydrogen bonding to the heme 6-propionate.

Presence of Sulfate in the SDH Active Site —Although sulfate is known to inhibit the catalytic activity of SDH and despite the fact that the crystallization medium contained 2.2 M sulfate in all cases, sulfate is not seen in the active sites of SDH^{WT}, SDH^{Y236F}, or SDH^{H57A} (11, 13). However, sulfate is present in the active site of SDH^{R55M}, where it appears to displace the

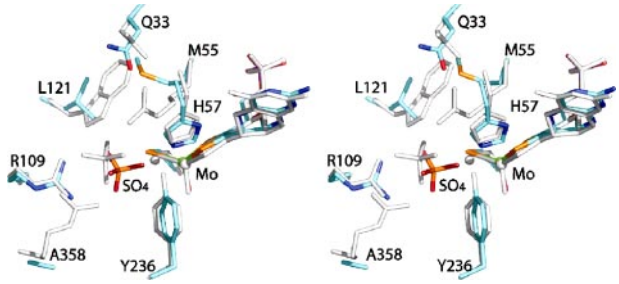

FIGURE 6. **Comparison of the position of bound sulfate in the active sites of SDH^{R55M} and CSO.** The *stereoview* shows the two active sites superimposed with the CSO residues *colored gray* and the the SDH^{R55M} atoms colored as follows: molybdenum (*green*), sulfur (*orange*), phosphorous (*magenta*), oxygen (*red*), nitrogen (*blue*), and carbon (*cyan*). *Labels* show residues with SDH numbering.

equatorial water/hydroxo ligand of the molybdenum as well as three solvent molecules that occupy the substrate-binding site in the wild type structure (Figs. 5 and 6). The sulfate anion interacts with Tyr-236 OH (2.7 Å), Arg-109 (two hydrogen bonds, 2.8 Å to NH1 and 2.9 Å to NH_2), the main chain nitrogen of Gly-106 (2.9 Å), Cys-104 Sγ (3.0 Å), and two water molecules (2.5 and 2.7 Å). One of the sulfate oxygen atoms is close to the position occupied by the equatorial water/hydroxo ligand in the SDH^{WT} structure, but the 3-Å distance from the molybdenum is too long for a direct molybdenum sulfate/sulfite bond.

Sulfate is found in the substrate binding site of all reported CSO crystal structures (10, 14). Although the position of sulfate in CSO is similar to that of the sulfate seen in SDH^{R55M}, a significant difference is that the equatorial oxygen on the molybdenum center is still present in the CSO structures, and the sulfate is rotated with respect to the sulfate in SDH^{R55M} so that none of the oxygen atoms is directed toward the molybdenum (Fig. 6). The presence of sulfate in the active site of SDH^{R55M} could be indicative of an increased inhibition of this enzyme by sulfate, and we explored this possibility by carrying out sulfate inhibition experiments with SDH^{WT} and SDH^{R55M}. Since $K_{m(\text{sulfite})(\text{app})}$ for SDH^{R55M} is extremely high (Table 3), investigations were carried out at pH 6 to allow the easy addition of excess sulfate to the assay mixture. Using standard assay conditions, increasing amounts of sodium sulfate (maximum of 80 mM) were added to the reaction mixture. For SDH^{WT}, plots of the reaction velocity *versus* the amount of sulfate present clearly show an exponential decay, with 50% inhibition occurring at an $I_{0.5\ \text{pH}\ 6}$ of 22.79 mM. In contrast, for SDH^{R55M}, the observed decrease of activity with increasing amounts of sulfate was much more linear and could be fitted equally well with a linear equation or an exponential equation. An $I_{0.5\ \text{pH}\ 6}$ value of 36.65 mM could be deduced from the exponential data fit. From this finding it appears as if SDH^{R55M} is in fact slightly less susceptible to sulfate inhibition than SDH^{WT}. However, this can be shown to be not necessarily true if the concentration of sulfate necessary to achieve 50% inhibition is expressed in terms of "excess over $K_{m(\text{sulfite})(\text{app})}$." For SDH^{WT}, 22.79 mM sulfate corresponds to $\sim 5.7 \times 10^4$ times $K_{m(\text{sulfite})(\text{app})}$, whereas for SDH^{R55M}, 36.65 mM sulfate corresponds to only about 40 times $K_{m(\text{sulfite})(\text{app})}$ of this enzyme, a difference of 3 orders of magnitude that clearly shows the higher susceptibility of SDH^{R55M} to inhibition by sulfate. Inhibition of both SDH^{WT} and SDH^{R55M}

by sulfate at pH 6 was investigated further by deriving the kinetic parameters for each enzyme at 0, 10, 30, and 60 mM sulfate present in the assay (data not shown). Analysis of this data revealed complex nonlinear responses in the inhibition that indicate the potential presence of multiple binding sites for sulfate as well as a pH-dependent change in the strength and type of the prevalent inhibition that is beyond the scope of this paper to discuss in detail.

DISCUSSION

Although enzymatic sulfite oxidation has been studied for more than 4 decades, the molecular details of this process are still not well understood. In all enzymatic catalysis, the formation of the enzyme-substrate complex and the breakdown of this complex into the reaction products are critical parameters, and our data presented above show for the first time how the three conserved active site residues Tyr-236, Arg-55, and His-57 shape the activity of sulfite-oxidizing enzymes by influencing these processes. Our data suggest that crucial factors in these processes are maintaining an optimal alignment of the active site environment and possibly facilitating electron transfer between the molybdenum and heme redox centers (11, 13).

Both Tyr-236 and Arg-55 are within Van der Waals contact distance of the molybdenum center and are hydrogen-bonded to the reactive equatorial oxo/hydroxo/water ligand. His-57 is located slightly further from the molybdenum. In all three cases, amino acid substitution led to marked changes in the alignment of the active site residues, particularly the position of the side chain of Arg-55 and in the catalytic activity of the resulting enzymes. Since no changes in the ligand environment of the heme c group were made and crystallography revealed few conformational changes around the heme iron atom, it is unlikely that the physical properties of this redox center have been altered as a result of the amino acid substitutions.

The kinetic data for SDH^{Y236F} suggest that Tyr-236 clearly affects enzymatic turnover, since the substitution decreases the turnover number of the SDH nearly 10-fold at the pH optimum of 8–9. The turnover numbers of SDH^{R55M} are also affected negatively and are only slightly higher than those of SDH^{Y236F}, although we note that it was only possible to measure SDH^{R55M} turnover reliably up to pH $\sim$ 8. We have identified a number of possible explanations for the reduction in catalytic activity that could apply to both substitutions. First, these effects could be mediated by the loss of the hydrogen bond from either Tyr-236 or Arg-55 to the equatorial oxo ligand of the molybdenum center. It is likely that these hydrogen bond interactions help stabilize the molybdenum center in an active state, since we see some loss of molybdenum in the structures of SDH^{R55M} and SDH^{Y236F} but not in wild type or His-57-substituted enzymes. Second, both structures identify a disruption of the salt bridge between Arg-55 and heme propionate-6, which may affect electron transfer between the two redox centers, although we note that the Mo–Fe distance of 16.6 Å may be close enough to allow electron "tunneling" to occur (35). Finally, we cannot rule out the possibility that the reduced activity is due to changes in the redox properties of the molybdenum atom, although we have so far failed to find evidence for such changes (13).

It is also interesting to note that in SDH^{WT} and SDH^{Y236F}, $k_{cat(app)}$ is clearly pH-dependent in a similar manner, whereas in SDH^{R55M} and SDH^{H57A}, $k_{cat(app)}$ values were steady from pH 6 to pH 8, with SDH^{H57A} exhibiting a single pK_a in the high pH range above pH 9. As expected by its greater proximity to the molybdenum center, the effect of the R55M substitution on enzymatic turnover is much more severe than that of the H57A substitution; however, in both cases, the pK_a value at pH 7.5 seen in the SDH^{WT} $k_{cat(app)}$ values is lost. The data imply that both His-57 and Arg-55 have a role in defining this low pH pK_a.

The R55M substitution also led to a significant increase in $K_{m(sulfite)(app)}$ by 2–3 orders of magnitude, which, in addition to the observed reduction in $k_{cat(app)}$ is probably exacerbated by changes in the formation rate of the enzyme-substrate complex and/or the rate at which the complex dissociates without catalysis having been achieved. These latter two effects would be specific to the R55M substitution, since SDH^{Y236F} shows a similarly reduced rate of turnover while maintaining a much higher substrate affinity. The less severe increase in $K_{m(sulfite)(app)}$ for SDH^{Y236F} and SDH^{H57A} may be at least partially due to disturbances in the position of Arg-55, since the crystal structures of both SDH^{Y236F} and SDH^{H57A} show that this residue is sensitive to its interactions with Tyr-236 and His-57. An entirely different and previously unobserved change in the pH dependence of $K_{m(sulfite)(app)}$ occurred in SDH^{H57A}; in all wild type and substituted SDH/SO enzymes studied so far, the affinity for the substrate increases at lower pH values, but in SDH^{H57A}, a minimum affinity for sulfite was reached at pH 7, indicating that His-57 is important in maintaining substrate affinity below pH 7, where the bulk of the substrate will be present in its protonated HSO_3^- form. At pH 7 and below, the His-57 imidazole ring should also be fully protonated, and the effect of His-57 on substrate binding may be exerted through its interactions with Arg-55.

Substitution of Arg-55 with methionine essentially creates an open space at the center of the SDH active site and disrupts the hydrogen bond network around the molybdenum and connecting the molybdopterin and heme redox centers. At the same time Arg-55 is also the innermost of the positively charged residues that line the active site channel of both SDH and CSO/HSO enzymes. There is evidence from the CSO structures that the arginine residues in the active site channel (Arg-138/55, Arg-190/109, and Arg-450,−; CSO/SDH numbering) are involved in achieving the correct orientation of the incoming sulfite molecule with respect to the molybdenum center (10).

The crystal structure of SDH^{R55M} is the only structure of SDH (11, 13) that has a sulfate molecule bound at the active site, despite the fact that the crystallization medium contains 2.2 M ammonium sulfate in all cases (Fig. 6). Modeling a sulfate molecule in the substrate binding site of SDH^{WT} in the same position and orientation as the sulfate in the SDH^{R55M} structure demonstrates that there is no clash with the position of the Arg-55 side chain and that two sulfate oxygen atoms are positioned to form hydrogen bonds with NE and NH_2 of Arg-55. However, the position and orientation of the sulfate molecule in the SDH^{R55M} active site is slightly different from that seen in

the CSO structures (10), since one of the sulfate oxygen atoms is positioned facing the molybdenum active site. Although the sulfate oxygen is too distant to actually bond to the molybdenum, it does appear to be able to displace the equatorial oxo/hydroxo/water ligand of the molybdenum center in the absence of Arg-55. We therefore propose that Arg-55 plays an important role not only in substrate binding, as demonstrated by our kinetic data, but also in product dissociation from the active site.

It is probable that the composition of the crystallization medium facilitates the formation of the sulfate complex seen in the crystal structure (Fig. 5*B*), which would be showing in effect a sulfate-inhibited form of the SDH. It seems less likely that the loss of the equatorial oxo/hydroxo/water ligand to the molybdenum center seen in the crystal structure is a permanent feature of SDH^{R55M}. A complete loss of the equatorial molybdenum ligand would be expected to have much more pronounced effects on catalysis, since this ligand is central to the formation of the enzyme-substrate complex. Pulsed EPR studies that are in progress, including ^{17}O labeling experiments, should provide important insight concerning the structure of the Mo(V) center of SDH^{R55M}.

It is not clear why the wild type and other substituted SDH structures do not have sulfate bound in the active site channel. One speculative possibility is the loss of a water molecule in the SDH^{R55M} structure, which hydrogen-bonds to Arg-55 NH2, Glu-33 OE1, and Gly-119 nitrogen in the wild type enzyme. This water is in a position that would allow it to hydrogen-bond to the substrate/product, and we propose a possible role in enzyme activity for this water molecule, which could displace the product sulfate from the molybdenum to become the water/hydroxo ligand of the reduced molybdenum redox center.

The changes seen in catalysis and the structure of SDH^{R55M} are also of interest, because this substitution is related to the R160Q substitution in the human sulfite oxidase (36), which is of clinical relevance and has been identified in an SO deficiency patient (14). In HSO, Arg-160 (Arg-138 in CSO) probably occupies a position equivalent to that of Arg-55 in SDH in the active site. Under standard assay conditions at pH 8, the $K_{m(\text{sulfite})(\text{app})}$ of HSO^{R160Q} was lowered by a factor of 100, and $k_{\text{cat}(\text{app})}$ was decreased by ~6.7 times relative to HSO^{WT} (36). The decreases in both values are nearly identical to those reported in this paper for SDH^{R55M}, suggesting that the kinetic effects of the R160Q and the R55M substitutions are quite similar. The sulfite oxidases from vertebrates are closely related, and the crystal structure of a R138Q-substituted CSO was recently reported (14). The structure showed a slightly altered position of Gln-138 compared with that occupied by Arg-138 in CSO^{WT} and small changes in the relative positions of Tyr-322 and Arg-190 (equivalent to Tyr-236 and Arg-109 in SDH), both located in the active site channel of the vertebrate sulfite oxidases (14). The major change observed in the CSO^{R138Q} active site, however, was a pronounced change in the position of the side chain of the outermost of the three arginines, Arg-450 (replaced by an alanine residue in SDH), which results in a narrowing of the active site entrance channel and was proposed to serve as a gating mechanism (14). Since this gating mechanism clearly cannot be functional in SDH, which lacks an Arg-450 equivalent, and in view of the similarity of the kinetic data for HSO^{R160Q} and SDH^{R55M}, it is unclear what influence the gating mechanism has on sulfite oxidation.

In summary, this work presents for the first time a comprehensive kinetic and structural analysis of the effect that the amino acid environment of the SO/SDH active site has on enzymatic catalysis. Substitution of Tyr-236 slows down enzymatic turnover significantly, whereas only a moderate effect on substrate affinity was observed. Our data indicate that Arg-55 is the most important of the three conserved active site residues, since it mediates substrate binding and product release as well as influencing turnover. SDH^{R55M} was the least catalytically competent (Fig. 3*F*) of the three substituted enzymes investigated here. We have also uncovered the previously unrecognized role of His-57 in substrate binding and low pH catalysis. Additionally, for SDH^{H57A}, the presence of two active site structural conformations and two distinct EPR forms raises the possibility of more than one catalytic pathway. The similarity of the SDH^{R55M} data to data previously reported for HSO^{R160Q} clearly shows the applicability of SDH-derived data for enzymatic sulfite oxidation in general.

Acknowledgment—We thank Dr. A. Raitsimring for helpful discussions concerning the EPR spectra.

REFERENCES

1. Kappler, U. (2008) in *Microbial Sulfur Metabolism* (Friedrich, C. G., and Dahl, C., eds) pp. 151–169, Springer, Berlin
2. Suzuki, I. (1994) *Methods Enzymol.* **243,** 447–454
3. Kappler, U., and Dahl, C. (2001) *FEMS Microbiol. Lett.* **203,** 1–9
4. Rajagopalan, K. V. (1980) in *Molybdenum and Molybdenum-containing Enzymes* (Coughlan, M. P., ed) pp. 243–272, Pergamon Press, Oxford
5. Hansch, R., Lang, C., Riebeseel, E., Lindigkeit, R., Gessler, A., Rennenberg, H., and Mendel, R. R. (2006) *J. Biol. Chem.* **281,** 6884–6888
6. Karakas, E., and Kisker, C. (2005) *J. Chem Soc. Dalton Trans.* **21,** 3459–3463
7. Feng, C., Tollin, G., and Enemark, J. H. (2007) *Biochim. Biophys. Acta* **1774,** 527–539
8. Enemark, J. H., and Cosper, M. M. (2002) *Met. Ions Biol. Syst.* **39,** 621–654
9. Mendel, R. R., and Bittner, F. (2006) *Biochim. Biophys. Acta* **1763,** 621–635
10. Kisker, C., Schindelin, H., Pacheco, A., Wehbi, W. A., Garrett, R. M., Rajagopalan, K. V., Enemark, J. H., and Rees, D. C. (1997) *Cell* **91,** 973–983
11. Kappler, U., and Bailey, S. (2005) *J. Biol. Chem.* **280,** 24999–25007
12. Kappler, U., Bennett, B., Rethmeier, J., Schwarz, G., Deutzmann, R., McEwan, A. G., and Dahl, C. (2000) *J. Biol. Chem.* **275,** 13202–13212
13. Kappler, U., Bailey, S., Feng, C. J., Honeychurch, M. J., Hanson, G. R., Bernhardt, P. V., Tollin, G., and Enemark, J. H. (2006) *Biochemistry* **45,** 9696–9705
14. Karakas, E., Wilson, H. L., Graf, T. N., Xiang, S., Jaramillo-Buswuets, S., Rajagopalan, K. V., and Kisker, C. (2005) *J. Biol. Chem.* **280,** 33506–33515
15. Schrader, N., Fischer, K., Theis, K., Mendel, R. R., Schwarz, G., and Kisker, C. (2003) *Structure* **11,** 1251–1263
16. Feng, C. J., Kedia, R. V., Hazzard, J. T., Hurley, J. K., Tollin, G., and Enemark, J. H. (2002) *Biochemistry* **41,** 5816–5821
17. Feng, C. J., Kappler, U., Tollin, G., and Enemark, J. H. (2003) *J. Am. Chem. Soc.* **125,** 14696–14697
18. Hille, R. (1996) *Chem. Rev.* **96,** 2757–2816
19. Ausubel, F. M., Brent, R., Kingston, R. E., Moore, D. D., Seidman, J. G., Smith, J. A., and Struhl, K. (2005) *Current Protocols in Molecular Biology*, John Wiley & Sons Inc., Hoboken, NJ
20. Kappler, U., and McEwan, A. G. (2002) *FEBS Lett.* **529,** 208–214
21. Ridge, J. P., Aguey-Zinsou, K. F., Bernhardt, P. V., Brereton, I. M., Hanson,

G. R., and McEwan, A. G. (2002) *Biochemistry* **41,** 15762–15769
22. Laemmli, U. K. (1970) *Nature* **227,** 680–685
23. Leslie, A. G. W. (1992) *Joint CCP4 and ESF-EACMB Newsletter on Protein Crystallography* **26,** Version 6.2.3, Medical Research Council, Cambridge, UK
24. CCP4 (1994) *Acta Crystallogr. Sect. D* **10,** 760–763
25. Jones, T. A., Zou, J. Y., Cowan, S. W., and Kjeldgaard, M. (1991) *Acta Crystallogr. Sect. A* **47,** 110–119
26. Murshudov, G. N., Vagin, A. A., and Dodson, E. J. (1997) *Acta Crystallogr. Sect. D* **53,** 240–255
27. Laskowski, R. A., Macarthur, M. W., Moss, D. S., and Thornton, J. M. (1993) *J. Appl. Crystallogr.* **26,** 283–291
28. Brody, M. S., and Hille, R. (1999) *Biochemistry* **38,** 6668–6677
29. Wilson, H. L., and Rajagopalan, K. V. (2004) *J. Biol. Chem.* **279,** 15105–15113
30. Astashkin, A. V., Enemark, J. H., and Raitsimring, A. M. (2006) *Concepts Magn. Reson. Part B* **29,** 125–136
31. Aylward, G. H., and Findlay, T. J. V. (1971) in *SI Chemical Data*, 1st Ed., pp. 122–123, John Wiley & Sons, Inc., New York
32. Dawson, R. M. C., Elliott, D. C., Elliott, W. H., and Jones, K. M. (1969) *Data for Biochemical Research*, 2nd Ed., Oxford University Press, Oxford
33. Enemark, J. H., Astashkin, A. V., and Raitsimring, A. M. (2006) *J. Chem Soc. Dalton Trans.* **29**, 3501–3514
34. Astashkin, A. V., Raitsimring, A. M., Feng, C. J., Johnson, J. L., Rajagopalan, K. V., and Enemark, J. H. (2002) *J. Am. Chem. Soc.* **124,** 6109–6118
35. Page, C. C., Moser, C. C., Chen, X., and Dutton, L. (1999) *Nature* **402,** 47–52
36. Garrett, R. M., Johnson, J. L., Graf, T. N., Feigenbaum, A., and Rajagopalan, K. V. (1998) *Proc. Natl. Acad. Sci. U. S. A.* **95,** 6394–6398
37. DeLano, W. L. (2002) *Pymol*, DeLano Scientific, Palo Alto, CA